Re-assessment of Al-Ce and Al-Nd Binary Systems Supported By Critical Experiments and First-Principles Energy Calculations

Michael C. Gao[1*], Necip Unlü[1], Gary J. Shiflet[1**]

Department of Materials Science and Engineering

University of Virginia, Charlottesville, VA 22904

Marek Mihalkovic[2], Michael Widom[2]

Department of Physics, Carnegie Mellon University

Pittsburgh, PA 15213

* Current contact address: Department of Materials Science and Engineering, Carnegie Mellon University, 5000 Forbes Ave., Pittsburgh, PA 15123. Email: mgao@andrew.cmu.edu.

** To whom all the correspondence should be addressed to: gjs@virginia.edu. Tel.: +1-434-982-5653; Fax.: +1-434-982-5660.

Abstract

The present study reinvestigates the Al-Ce and Al-Nd phase diagrams and reoptimizes the thermodynamics via the CALPHAD method. First-principles energy calculations play an important role in terms of sublattice formalism and phase stability prediction, demonstrating that they

should be effectively integrated into experimental investigation and thermodynamic assessment. Specifically, our experimental results and theoretical calculations show that Al_2Nd (or Al_2Ce) should be treated as a stoichiometric compound phase rather than the solution phase that was proposed in previous studies.[18-20] Further, we find that a new compound $AlCe_2$ is stable at high temperatures (648-775^{o}C) in the Al-Ce system. It forms by peritectic reaction of liquid and AlCe phases at 775^{o}C, and decomposes into AlCe and $\beta AlCe_3$ at 648^{o}C and below. Since the $AlCe_2$ phase is not retained at room temperature by quenching experiments, we suggest that $AlCe_2$ may be isostructural with the previously known compound $AlNd_2$ (oP12). Based on our DTA measurement and theoretical calculations, we also propose that there is a α/β-Al_3Ce polymorphous transition occurring at 973^{o}C in Al-Ce system and a α/β-Al_3Nd polymorphous transition occurring at 888^{o}C in Al-Nd stem. The β-Al_3RE phase may be isostructural with β-Al_3Y (hP12). Finally, we propose that the so-called β-$Al_{11}RE_3$ phase (RE=La,Ce,Nd,Pr)[7,8,21,22] should have a stoichiomestry of Al_4RE (tI10), based on direct evidence from our DSC measurement.

1. Introduction

Due to their promise in engineering applications and fundamental scientific interest, research in metallic glasses (MG) has grown recently. In particular, Al-based MG[1,2] receive great attention due to their high specific strength. Glass formation can be achieved on both the Al-rich and RE-rich sides for Al-RE systems (RE = rare earth elements). Similar glass formation

phenomena occur in Al-TM-RE ternary systems[1,2] (TM = transition metals). Glass formation is difficult in the Al-rich corner while bulk MG form in the RE-rich corner with a slow cooling rate. We believe that the underlying thermodynamics plays an important role in amorphourization during a quench. Accurate phase diagrams and reasonable thermodynamic parameters for all the equilibrium and metastable phases, must be determined consistently. Consequently, we are investigating the Al-Co-Ce and Al-Ni-Nd systems in their Al-rich corner, integrating critical experiments, first-principles energy calculations and CALPHAD modeling. To begin, we present our results on the Al-RE binaries.

A number of authors experimentally investigated and thermodynamically studied and assessed the Al-Ce and Al-Nd binary systems.[3-26] Detailed reviews and bibliographic information can be found in refs.[11,18,21,22] Cacciamani *et al.* performed a recent assessment,[18,20] in which they modeled the compound phase Al_2Nd (or Al_2Ce, cF24) as a 2 sublattice solution phase in which Al and Ce (or Nd) atoms can mix with each other in each sublattice (see Figure 1). In this model, both Al_2Nd and Al_2Ce exhibit appreciable solubility ranges at high temperatures, but experimental evidence is absent. In the present study, such a solution trend in cF24 (if any) is analyzed using first-principles energy calculations and thermal analysis measurements. Further, thermal measurements were performed for the whole Al-Ce binary and the Al-rich Al-Nd systems, and we report some new phases, namely $AlCe_2$ (oP12), β-Al_2Ce (hP12) and β-Al_2Ce (hP12), which are stable in the systems we studied. In this study, first-principle energy calculations were successfully integrated into our experimental investigation and Calphad modeling, and we suggest that such integration should be applied extensively into phase diagram research.

Based upon our first-hand experimental data, supported by theoretical prediction together with literature information, both the Al-Ce and Al-Nd systems were thermodynamically optimized using the PARROT module of the commercial Thermo-Calc software.[27]

2. Experimental Procedures and Results

All alloys were synthesized through arc-melting pieces of Al (99.999% purity, all are in atomic percentage unless specified otherwise) and Nd (99.9%) or Ce (99.9%) on a water-cooled copper hearth using a tungsten electrode in an argon atmosphere. The ingots, about 2-5 grams, were remelted 4~5 times to insure chemical homogeneity, and cooled to room temperature inside the arc furnace. The weight loss is about 1wt%. Differential thermal analysis (DTA) was performed on all the as arc-melted samples. The DTA measurement was originally performed using a PerkinElmer DTA7 for several alloys at a heating/cooling rate of 10K/min, and later using a Netzsch DSC404C with a DTA carrier at a heating rate of 20^{o}C/min that has much better capability in terms of preventing oxidation with a turbo pump. In fact, the sample chamber of the DSC404 was initially evacuated to high vacuum to about 1.0x10^{-5} torr and then backfilled with flowing high-purity argon (grade 5). The Netzsch DTA carrier was calibrated with 7 standards including Sn, Bi, Zn, Al, Ag, Au and Ni so that the measurement would be accurate over a wide temperature ranges. The overall accuracy of the DTA measurement is $\pm$3 ^{o}C over the temperature range of 100-1600^{o}C. A typical DTA plot is shown in Fig. 2 for alloys $Al_{97.4}Ce_{2.6}$ and

$Al_{82.5}Ce_{17.5}$. Some samples were also analyzed using a PerkinElmer DSC7 and the Netzsch DSC404.

Figure 3 shows the DTA plot for 4 alloys, namely (a) $Al_{40}Ce_{60}$, (b) $Al_{30}Ce_{70}$, (c) $Al_{20}Ce_{80}$ and (d) $Al_{25}Ce_{75}$, during the heating segment. Three main thermal events occur in $Al_{40}Ce_{60}$ (Fig. 3a). The first corresponds to decomposition of β-$AlCe_3$ into AlCe and $AlCe_2$ at ~648°C; the second is the peritectic melting of $AlCe_2$ into AlCe and liquid at ~775°C; the third is the peritectic melting of AlCe into Al_2Ce and liquid at ~855°C. The final melting signal is very weak and the liquidus temperature is estimated as 958°C. Alloy $Al_{45}Ce_{55}$ exhibits a very similar DTA plot as $Al_{40}Ce_{60}$, namely 3 main peaks that occur at temperatures almost identical to $Al_{40}Ce_{60}$, plus a final melting peak. Such identical thermal history for both alloys indicate that they must be chemically located at the same phase field. Note that the second thermal event for both alloys was not reported in the literature, and perhaps this is reason why $AlCe_2$ was not identified. Only 2 main thermal events occur in $Al_{30}Ce_{70}$ (Fig. 3b). The first peak is broad and is believed to contain 2 overlapping reactions, i.e., $\beta AlCe_3 + AlCe \leftrightarrow AlCe_2$ and $\beta AlCe_3 \leftrightarrow AlCe_2 + Liquid$. The second event has a well-defined onset at ~778°C, which is almost identical to the onset of the second thermal event of alloys $Al_{40}Ce_{60}$ and $Al_{45}Ce_{55}$ within the experimental error range. Based upon the DTA measurements of these 3 alloys, the peritectic reaction of $AlCe + Liquid \leftrightarrow AlCe_2$ at ~775°C can be reasonably justified. The perectic point is estimated to be slightly richer in Ce than $Al_{30}Ce_{70}$ whose final melting point is about 802°C. Note that $Al_{30}Ce_{70}$ was reported as the eutectic point of the reaction $Liquid \leftrightarrow AlCe + \beta AlCe_3$,[8] while

the same reaction was reported to occur at a composition of $Al_{27.5}Ce_{72.5}$.[17] Alloy $Al_{20}Ce_{80}$ (Fig. 3c) has 2 main (slightly overlapping) peaks and a final shallow melting peak. The first peak is the eutectic reaction of $Liquid \leftrightarrow \gamma Ce + \beta AlCe_3$ occurring at 590°C, and the second peak is believed to be the peritectic reaction of $AlCe_2 + Liquid \leftrightarrow \beta AlCe_3$. The peritectic point is estimated as slightly over the composition $Al_{20}Ce_{80}$. The first peak of alloy $Al_{25}Ce_{75}$ (Fig. 3d) appears sharp but actually it consists of two overlapping peaks (it is magnified in Fig. 3e). This implies that the bulk alloy chemistry is slightly off its norminal value. But a more important conclusion is that the reaction $AlCe_2 + Liquid \leftrightarrow \beta AlCe_3$ occurs at a just slightly higher temperature than that of $\beta AlCe_3 + AlCe \leftrightarrow AlCe_2$ at 647°C, and that these two temperatures are almost too close for DTA to differentiate clearly. In summary, our DTA measurements on the Ce-rich alloys supports that there is a new phase $AlCe_2$, stable at a narrow temperature range of 648-775°C. Note that $Al_{25}Ce_{75}$ was reported to melt congruently at 655°C by Buschow *et al.*,[8] which is fairly close to our value. On the other hand, Saccone *et al.* reported that $Al_{25}Ce_{75}$ melted congruently at 685°C,[17] but they also reported another peak at 600°C for this alloy.[17]

Figure 4a shows the DSC plot for alloy $Al_{11}Nd_3$ at a heating rate of 20K/min. The presence of a very small peak occurring at ~641°C with a heat of 0.83J/g, indicating its bulk chemistry is slightly shifted towards Al-rich side; it corresponds to the eutectic reaction of $Liquid \leftrightarrow Al + Al_{11}Nd_3$. The second peak occurs at a sharp onset of 926°C and with a heat of of 12.9J/g; it corresponds to the reaction of $Liquid + Al_{11}Nd_3 \leftrightarrow Al_4Nd$. The third peak is shallow with an estimated onset of 963°C and a heat of 2.3J/g; it corresponds to the reaction of

$Al_{11}Nd_3 \leftrightarrow Al_4Nd + \beta Al_3Nd$. These two thermal events directly supports our idea that the so-called β–$Al_{11}RE_3$ [7,8,21,22] should be chemically treated as Al_4RE (RE=La,Ce,Nd,Pr) phase; a single α/β-$Al_{11}RE_3$ polymorphous transformation just cannot explain both the 2nd and 3rd thermal events. This idea gains further support from theoretical calculation described in section 3. The 4th peak occurs at 1216°C with a very large amount of heat (181J/g). However, its first derivative (shown in the inset) indicates it may consist of two peaks, which in fact correspond to the reactions of $Al_2Nd + Al_4Nd \leftrightarrow \beta Al_3Nd$ and $Al_2Nd + Liquid \leftrightarrow Al_4Nd$ (these 2 reactions become less overlapping in Fig. 4b for alloy $Al_{76}Nd_{24}$). The final liquidus is estimated at 1275°C, which corresponds to the melting of Al_2Nd. Based upon the above information, we think this alloy $Al_{11}Nd_3$ (Fig. 4a) must chemically lie between $Al_{11}Nd_3$ and Al_4Nd, and is fairly close to Al_4Nd. For this alloy, the heat from the reaction $Al_2Nd + Al_4Nd \leftrightarrow \beta Al_3Nd$ is negligible, and the large heat (or enthalpy change) seen in the 4th peak (Fig. 4a) is contributed mainly from the peritectic melting of Al_4Nd. Figure 4b shows the DTA plot of alloy $Al_{76}Nd_{24}$ at a rate of 10K/min using a PerkinElemer DTA 7. The first thermal event occurs at 888°C (indicated by the arrow), and we think it may correspond to the α/β-Al_3Nd phase transition. The reaction of $Al_{11}Nd_3 \leftrightarrow Al_4Nd + \beta Al_3Nd$ is not detected in the DTA scan, and the reason can be due to small amount of heat and slow kinetics for this reaction. Figure 4c shows the DTA plot of alloy $Al_{75}Ce_{25}$ done with a PerkinElmer DTA 7 with a heating/cooling rate of 10 K/min. The first thermal event shown in the heating segment corresponds to the α/β-Al_3Ce polymorphous phase transition occurring at ~973°C. Such thermal event is also observed in alloys $Al_{77}Ce_{23}$ and $Al_{77}Ce_{30}$ on their DTA scan (their DTA plots are not shown here, refer to Fig. 7 for the DTA data points).

Based on these DTA measurements, we think β-Al_3Ce and β-Al_3Nd can be high-temperature stable phases, whose crystal structure is proposed to be isostructural of Al_3Y (hP12).

In order to verify the existence and its crystal structure of $AlCe_2$ and the polymorphous transformation of $AlCe_3$ at 250°C,[5] we chose two samples, $Al_{45}Ce_{55}$ and $Al_{40}Ce_{60}$, for heat treatment at 700, 500 and 200°C for 10 days, respectively, followed by quenching in cold water. These samples were encapsulated and sealed inside silica tubes under a partial pressure of argon. As heat-treated samples were ground with a series of SiC paper and polished using diamond paste, and finally examined in a JEOL 6700-scanning electron microscopy (SEM) for microstructure analysis. Electron probe Microanalysis (EPMA), using pure element samples as external standards, was employed to perform all the chemical analysis. The accuracy of the EPMA measurement in this study is about 1 at%.

The polymorphous transformation of α/β-$AlCe_3$ occurring at 250°C[5] was not detected by DTA measurement in this study. We also used a PerkinElemer differential scanning calorimetry (DSC7) that has much higher sensitivity to analyze some samples at a rate of 20K/min, but no signal was detected at 250°C either. The polymorphous transformation of α/β-$AlCe_3$ is confirmed in our microstructure analysis, but the exact transformation temperature is not confirmed. Figure 5a, 5b, 5c, respectively, show the microstructure of alloy $Al_{40}Ce_{60}$ after annealing at 700°C, 500°C and 200°C for 10 days. Three phases were present in Fig. 5a and 5b, namely AlCe, α-$AlCe_3$ and β-$AlCe_3$. Note $AlCe_2$ is not retained in Fig. 5a, indicating the fast kinetics in its decomposition during quenching. No β-$AlCe_3$ was detected in Fig. 5c as expected. The micro-

structure of alloy $Al_{45}Ce_{55}$ after annealing at 700°C, 500°C, 200°C, was found to be very similar to those in alloy $Al_{40}Ce_{60}$ (results not shown here). Both alloys remained intact in shape after annealing at 700°C for 10 days, demonstrating that melting did not occur at 700°C for these 2 alloys. However, according to the previously reported phase diagrams[8,17], both alloys should have melted into liquid+AlCe at 700°C. Therefore, we conclude that the phase $AlCe_2$ must appear as stable at a narrow temperature range of 648-775°C, whose crystal structure is predicted to be isostructural of previously know compound $AlNd_2$ (oP12) (see the next section for details).

3. First-principle energy calculations

Our first-principles calculations employ the plane-wave code VASP,[28,29] which solves for the electronic band structure using electronic density functional theory. Because of the presence rare-earth elements Ce and Nd, we use PAW potentials[30] as supplied with VASP. These are similar to pseudopotentials except that the core levels are solved simultaneously with the valence electrons. We treat the entire f-levels within the valence band and use the PBE gradient approximation[31] to the exchange-correlation functional. Reciprocal space (k-point) meshes are increased to achieve convergence to a precision of 10 meV/atom. All structures are fully relaxed (both lattice parameters and atomic coordinates) until, again, energies converge to a precision of 10 meV/atom. The plane-wave energy cutoff was held constant at 300 eV for Al-Ce and 253 eV for Al-Nd, the defaults for the rare-earth potentials. All calculations were performed using the

‘‘Accurate’’ setting which avoids wrap-around errors. Spin polarization was considered in all calculations other than pure Aluminum. To obtain enthalpy of formation values ΔH_{for}, we subtract a composition-weighted average of the pure elemental cohesive energies from the cohesive energy of a given compound. The resulting energy is an “enthalpy” because its volume was relaxed (at zero pressure). It is at T=0K because its atomic coordinates are relaxed.

Vertices of the convex hull of a scatter plot of ΔH_{for} versus composition identify stable structures. Points above the convex hull represent thermodynamically unstable structures, though they may be metastable or high temperature stable in some cases. Most of the structures we examined were mechanically stable, in the sense that atomic displacements during relaxation were generally small (less than 0.3A at worst). The Al_4La.oI30 type structures had large displacements because the starting crystallographic structure is not good. Details of the relaxed structures can be found on the WWW.[32]

Resulting enthalpies of formation are displayed in Fig. 6, and the enthalpy value is listed in Table 1. Our plotting symbol notation is: heavy circles for known stable binary phases; light circles for known high temperature phases; diamonds for known metastable phases; triangles for known high pressure phases; squares for imperfectly known, unknown or hypothetical structures. Tie-lines run along convex hull edges, joining low enthalpy structures at the vertices of the convex hull. Structures are labeled using the notation {prototype}.{Pearson} where the prototype is the name of some commonly known isostructural compound, and the Pearson symbol gives point symmetry, translational symmetry and number of sites per unit cell. For example, the structure in

the Al-Ce binary diagram (Fig. 6a) labeled $AlNd_2$.oP12 contains Al and Ce atoms arranged as in $AlNd_2$ with Ce substituting for Nd. This structure is orthorhombic, primitive (no centering) with a twelve atom unit cell.

The binary phase diagrams are fairly well reproduced, but the overall level of agreement is lower than we have found in similar studies of compounds not containing rare earth elements.[33] The experimental phase diagrams of Al-Ce and Al-Nd are quite similar to each other, as are our calculated results. The following discussion addresses Al-Ce and Al-Nd simultaneously, starting from pure Al and ending with pure RE. For pure Al we compared FCC (cF4), HCP (hP2) and BCC (cI2) structures, finding the known FCC structure favored.

The low temperature stable α-$Al_{11}RE_3$.oI28 phases are on the convex hull for Al-Nd and just 2 meV/atom above for Al-Ce. The high temperature β phases with Pearson symbol tI10 lie above the convex hulls by about 40 meV/atom in each case. According to the experimental phase diagrams the composition of β matches that of α,[7,8,18] but the ideal composition of tI10 is more Al-rich than oI28. We found that introducing an Al vacancy on the 4e site of tI10 raised the energy by an additional 40 meV/atom (i.e. 400meV/vacancy) above the convex hull. Other sites were even more unfavorable. In the current thermodynamic modeling, the so-called β-$Al_{11}RE_3$ phase is corrected as stoichiometric Al_4RE compound. Reports[34] of Al_4RE phases with structure type oI30 (prototype Al_4La) are highly doubtful because we find their enthalpies of formation are positive. There is thus no driving force to create such a crystal structure from its constituent

elements.

The next two phases, Al_3Ce.hP8 and Al_2Ce.cF24 are correctly placed on the convex hull. As a candidate for the previously unreported structure β-Al_3Ce/β-Al_3Nd, we considered the prototype Al_3Y.hR12. At ΔE of around 20 meV/atom, this could easily arise as a high temperature phase. As suggested by Cacciamani and Ferro[18] (see Fig. 1) we explored the possibility of sublattice mixing in the cF24 structures. To test this possibility we investigated compositions $Al_{(1-x)}RE_x$ (x=0.292, 0.333 and 0.375) by taking a 24-atom unit cell of Al_2RE.cF24 and replacing a single atom with one of the opposite type. We found energy costs around 1 eV for each replacement. Estimating entropy gains upon replacement from the numbers of available sites yields temperatures exceeding 4000K at which sublattice disorder should be important. Since this temperature greatly exceeds the melting temperature we conclude that sublattice mixing can safely be ignored in these alloy systems.

For the RE-rich portions of the phase diagrams we find numerous small disagreements between calculation and experiment. We believe this indicates imperfect treatment of rare-earth atoms by our calculations methods. Some specific shortcomings are: (1) use of an approximate exchange-correlation potential while tightly bound f-electrons may exhibit strong correlations; (2) use of non-relativistic equations for high atomic number elements; (3) assumption of collinear magnetism while rare-earths often exhibit noncollinear magnetism.

At composition x=0.5, both experimental phase diagrams show stable phases. In both

cases our calculations find these phase lie slightly above the convex hulls. In the case of Al-Nd we incorrectly find the AlCe.oC16 structure lower in energy than AlNd.oP16. At composition x=0.667, both calculations find the $AlNd_2$.oP12 experimentally structure slightly above the convex hull. This structure is known to be stable even at low temperatures in Al-Nd. We predict that the observed high temperature stable compound $AlCe_2$ should be isostructural to $AlNd_2$. A reported[34] metastable phase $AlNd_2$ of structure cF24 has positive enthalpy of formation and is probably an incorrect report.

At composition $AlCe_3$, the established phase diagram shows a sequence of phases, mC16, hP8 and cP4 at progressively higher temperatures. Our energy data reproduces this sequence, but we find even the lowest energy lies slightly above the convex hull. In the case of Al-Nd, we correctly find that $AlNd_3$.hP8 touches the convex hull.

Pure elemental Ce exhibits a complicated sequence of structures as temperature rises, α (FCC, low volume), β (cP4), γ (FCC, high volume), δ (BCC). Because we relax the cell volume, we are not able to find the high volume γ phase, but the others (α, β and δ) are properly ordered in enthalpy. Likewise the high pressure phases lie correctly above the alpha phase in enthalpy. Although we considered spin polarization, our calculations for pure Ce did not find spin polarized states, probably because the actual magnetic structures are spin canted in various manners. Pure elemental Nd exhibits only two phases, α(hP4) and β(BCC). Our calculations place these in the proper sequence, and find the high pressure FCC structure properly above α.

4. Thermodynamic model

The Gibbs free energy of individual phases is described by sublattice models[35] and is defined relative to the Stable Element Reference (SER), i.e., the enthalpies of the pure elements in their defined reference phase at 298.15K and 1 atm. All the disordered solutions including liquid were modeled with a single sublattice, with the Gibbs energy expressed as for a binary phase with components A and B:

$$G^{\phi} = x_A {}^{o}G_A^{\phi} + x_B {}^{o}G_B^{\phi} + RT(x_A \ln x_A + x_B \ln x_B) + {}^{E}G^{\phi} + {}^{mg}G^{\phi}.$$

where ${}^{o}G_i^{\phi}$ is the molar Gibbs energy of the pure element *i* in the structure of phase ϕ in the non-magnetic state, taken from the values tabulated by Dinsdale[36], and x_i is the mole fraction of each component. The excess Gibbs energy is expressed in Redlich-Kister-Muggianu polynomial form [37, 38]:

$${}^{E}G^{\phi} = x_A x_B \sum_i {}^{i}L_{\mathrm{A,B}}^{\phi}(x_A - x_B)^{i} \quad .$$

${}^{i}L_{A,B}^{\phi}$ are the binary interaction parameters evaluated in the present work, which is typically modeled as: ${}^{i}L = {}^{i}a + {}^{i}bT + {}^{i}cT\ln(T) + {}^{i}dT^2$. The magnetic contribution to the Gibbs energy for all binary compound phases was set to zero due to lack of experimental data.

Stoichiometric compounds are modeled as if the enthalpy and entropy are constants and only one element occupies one sublattice. For example, the Gibbs free energy for a binary stoichiometric compound A_xB_y is modeled as (J/g-atom):

$$G^{A_xB_y} = \frac{x}{x+y}{}^{o}G_A + \frac{y}{x+y}{}^{o}G_B + a + bT.$$

5. Optimization results and discussion

The present optimization is primarily based on the experimental data from this study and those available from the literature. For our DTA analysis, only the data from the heating segment are taken and the cooling segment is only used to assist DTA analysis. This is because DTA or DSC is always calibrated using the onset temperature during the melting process of high-purity standards. All the invariant reactions are characterized by their onset temperatures, and the liquidus temperatures are estimated by the final peak temperature. Further, it is found that Ce and Nd-rich alloys are prone to oxidation, especially in the liquid state. Therefore, the liquidus temperatures are set with lower weight during optimization with respect to the invariant reaction temperatures that are seen to be reproducible and thus more reliable.

Our experiments show that there is a new compound phase stable only at high temperatures (648-755^{o}C) in the Al-Ce system, and we have proposed it is $AlCe_2$ (oP12). The first-principle energy calculations show that it is just slightly above on the convex hull at 0K, and can easily become stable at high temperatures. From our DTA measurements we see a high probability of α/β-Al_3Ce polymorphous transition occurring at 973^{o}C in Al-Ce system and one of α/β-Al_3Nd transition occurring at 888^{o}C in Al-Nd system. We have proposed the β-Al_3RE phase may

be isostructural of the previously reported compound Al_3Y (hP12), and the first-principles energy calculations again show that β-Al_3RE (hP12) is very likely stable at high temperatures. The Al_4RE (tI10) phase has been long been treated as β-$Al_{11}RE_3$ (tI10) under the assumption of Al deficiency via vacancy mechanism. First-principles energy calculations show that vacancy substitution for Al sites is energy costly and thus such claim is physically unlikely. Indeed, our DSC measurement on alloy $Al_{11}Nd_3$ (norminal composition, its real chemistry may be close to $Al_{79.5}Nd_{20.5}$) resolved that $Al_{11}Nd_3$ (oI28) can be formed by catetectic reaction $Liquid + Al_{11}Nd_3 \leftrightarrow Al_4Nd$ and eutectoid reaction of $Al_{11}Nd_3 \leftrightarrow Al_4Nd + \beta Al_3Nd$. The former is associated with a large amount of heat and fast kinetics due to involvement of the liquid phase, and thus can be easily detected by DTA and shown as a sharp peak in the DTA plots. In contrast, the latter is associated with a small amount of heat and perhaps the kinetics is relatively slow, thus it can only be detected by DSC measurement. Further, the invariant temperatures for these 2 reactions are fairly close so that they can be misinterpreted easily. Although direct microstructure evidence is not achieved in this study, an in situ x-ray diffraction or in situ transmission electron microscopy would help to confirm its chemistry and crystal structure. Further, for alloys (such as $Al_{65}Ce_{35}$) that are close to Al_2Ce, our DTA measurement does not support the phase diagram[18] since the solidus and the solvus was not detected. In fact, our energy calculations predict that substitution between Al and RE atoms for Al_2RE compounds can only occur at a temperature that is much higher that its congruent melting point. Therefore, it is physically reasonable to model it as a stoichiometric phase.

We find most of our DTA measurements agree with those in the previous reports[5,8,9,10,17,21] except the reaction $Al_4Ce + Al_2Ce \leftrightarrow \beta Al_3Ce$, which occurs at 1192°C, but was reported to occur at 1135°C.[8] We also find the eutectic reaction in the very Al-rich side occurs at 641°C with a eutectic point of ~2.6 at% Ce (see Fig. 2a). This eutectic point was reported as 4.0at% Ce at 640°C,[8] and 2.6% Ce at 633°C.[10] Al_4Ce decomposes into liquid and $Al_{11}Ce_3$ at 1006°C. $Al_{11}Ce_3$ is formed eutectoidly from Al_4Ce and β-Al_3Ce, and the transformation temperature is not identified in this study and is proposed to be at 1020°C, the α/β-$Al_{11}Ce_3$ transition temperature originally reported by Buschow.[8] Al_2Ce is found to melt congruently at 1455°C, while it was reported as 1480°C.[8] We find the reaction $Liquid + Al_2Ce \leftrightarrow ACe$ occurs at ~855°C, while it was reported at 845°C. But, a small flucturation on this transition temperature was seen in this study. The eutectic point of $Liquid \leftrightarrow \beta AlCe_3 + \gamma Ce$ is found to be 90at% Ce at 590°C. This finding is closer to what was reported as 89at% Ce at 580°C[8], than what was reported as 86 at% Ce at 600°C.[17]

Based upon our measurement and other literature information, the Al-Ce system is optimized using PARROT module. The thermodynamic parameters that were determined in this study for Al-Ce system are listed in Table 2. The calculated Al-Ce phase diagram is shown in Fig. 7, and the experimental data including invariant reaction and liquidus temperatures obtained from this study and the literature are shown for comparison. It is seen that the computed Al-Ce phase diagram agrees very well with DTA data points, and an excellent agreement for all the invariant

reactions is achieved. On the other hand, agreement of the computed liquidus boundary is good overall but less satisfactory, and we think this may be due to (1) the intrinsic uncertainty in terms of liquidus measurement; (2) lack of sufficient reliable thermodynamic measurement of liquid phase; (3) the high susceptibility to oxidation for RE-rich alloys. Fig. 8a plots the enthalpy of mixing at 300K with experimental data on enthalpy formation of compound phases at 300K and the ones calculated from the first principles. The optimized enthalpy formation of all the compound phases agree very well with the ones determined experimentally whose error is about 2-3kJ/g-atom.[25,26] On the other hand, the ones calculated from the first principles agrees reasonably well with the experimental ones for Al_4Ce, $Al_{11}Ce_3$ and Al_2Ce only. A large discrepancy for AlCe, $AlCe_2$ and $AlCe_3$ is obvious, and is probably due to the previously-mentioned difficulties of treating rare-earth elements. Figure 8b shows total enthalpy as a function of temperature for 2 alloys, namely, $Al_{70}Ce_{30}$ and $Al_{40}Ce_{60}$. All the first-order phase transitions are recognized by the discontinuity of the total enthalpy at the transition temperature that are marked by the vertical dotted lines. The calculated enthalpy change for α/β-$AlCe_3$ polymorphous phase transformation in $Al_{40}Ce_{60}$ is ~0.1 kJ/mole of atoms. This calculated value is very reasonable in the sense that this transformation was not detected by DSC probably because the enthalpy change is so small; Our quenching experiments showed that the kinetics is actually very fast for the α/β-$AlCe_3$ transformation. For all the invariant reactions, we further find that the calculated enthalpy change is in very good agreement with those obtained from DTA measurement (obtained by the integrated area under the peak in the DTA plot) (see Fig. 3a), given the fact that the error in DTA enthalpy measurement is typically ~20%. Similar conclusion can be drawn for alloy $Al_{40}Ce_{60}$ and other

Al-Ce alloys.

Concerning the Al-Nd system, DTA measurement was performed on 7 Al-rich alloys. We find a eutectic reaction $Liquid \leftrightarrow Al + Al_{11}Nd_3$ occurs at 641°C, and $Al_4Nd \leftrightarrow Liquid + Al_{11}Nd_3$ occurs at 934°C. The thermodynamic parameters that were determined in this study for Al-Nd system are listed in Table 3, and the calculated Al-Nd phase diagram is shown in Fig. 9 with all the DTA data points marked for comparison. Again, an excellent agreement between our calculated invariant reactions with the ones determined experimentally is achieved except the liquidus of the Nd-rich part. The $AlNd_3$ phase was reported to melt peretectically at 675°C,[7] and at 780°C.[17] Saccone *et al.*[17] also proposed a eutectoid reaction of $\beta Nd \leftrightarrow \alpha Nd + AlNd_3$ at 650°C, and a eutectic reaction of $Liquid \leftrightarrow \beta Nd + AlNd_3$ at 690°C with a eutectic point of 81 at%Nd. We find that the reactions $AlNd_2 + Liquid \leftrightarrow AlNd_3$ and $Liquid \leftrightarrow \beta Nd + AlNd_3$ together with very narrow temperature range of the phase field of liquid+$AlNd_2$ cannot be fulfilled simultaneously. Indeed, in Cacciamani's assessment,[18] the reaction $Liquid \leftrightarrow \beta Nd + AlNd_3$ was optimized to occur at 727°C (37°C higher than the experimental value[17]) with a eutectic point of 82.8at% Nd. In our assessment, $AlNd_2$ melts congruently. All the nearby invariant reaction temperatures are excellently fulfilled. The calculated heat of mixing for Al-Nd alloys at 300K and the measured enthalpy of formation for Al-Nd compound phases at 300K are presented in Fig. 10a, and the agreement with the experimental values is excellent within the experimental errors. As was the case in the Al-Ce binary system, the values calculated from the first principles on the other hand agree reasonably well with experimental

ones only for the Al-rich compounds, namely, Al_4Nd, $Al_{11}Nd_3$ and Al_2Nd. For the Nd-rich compounds, the calculated values are significantly higher (towards more positive direction) than the experimental ones. Figure 10b shows total enthalpy as a function of temperature for 2 compositions, namely, $Al_{79.5}Nd_{20.5}$ and $Al_{76}Nd_{24}$. $Al_{79.5}Nd_{20.5}$ was chosen because we believe that our alloy $Al_{11}Nd_3$ may have a real chemistry close to this composition. If compared with the enthalpy change obtained from DSC/DTA measurement (see Fig. 4), we find all the calculated ones are very reasonable, although there is no experimental report on the enthalpy of formation of the Al_4Nd phase.

In the present study, the first-principles energy calculations have been helpful in verifying the sublattice model of Al_2RE (cF24) phase, predicting the stability of the $AlCe_2$ (oP12) and β-Al_3RE (hP12) phases, whose microstructure evidence are not available, and examining the phase relationship between Al_4RE and $Al_{11}RE_3$. All these theoretical results provide confidence in our experimental investigation, validating a CALPHAD model that is physically grounded. Further, the enthalpy of formation for compound phases directly calculated from the first principles can be directly integrated into the CALPHAD methodology. Such integration will become valuable in cases where such experimental information is absent. Further, it decreases the number of variables to be optimized, thus improve the accuracy of CALPHAD modeling in principle. In fact, such ideas have been implemented by Kaufman *et al.*[40] to predict the Cr-Ta-W ternary phase diagram and by Wolverton[41,42] to study phase metastability and phase equilibrium in commercial Al alloys.

6. Conclusions

We re-investigated the Al-Ce and Al-Nd systems using first-principles energy calculation and critical experiments, reaching the following new conclusions: (1) An equilibrium phase $AlCe_2$ exists and is stable at high temperatures (647-775^oC). Its structure is probably oP12. (2) The so-called β-$Al_{11}RE_3$ (RE=La,Ce,Nd,Pr) should ideally have a stoichiomestry of Al_4RE (tI10). (3) There exist a α/β-Al_3Ce polymorphous transition occurring at 973^oC in Al-Ce system and a α/β-Al_3Nd polymorphous transition occurring at 888^oC in Al-Nd system. The β-Al_3RE phase may be isostructural with β-Al_3Y (hP12). (4) The cF24 structures of Al_2Ce and Al_2Nd should be treated as stoichiometric compound phases. (5) α/β-$AlCe_3$ polymorphous transition is confirmed, but the exact transition temperature (between 200-500^oC) is not identified. (6) The invariant temperatures detected during the heat segment were emphasized during optimization rather than the liquidus temperatures. The former are always easier to identify during thermal analysis and thus are of high accuracy and reproducibility. Therefore, they should be assigned high weight during optimization. (7) Both the Al-Ce and Al-Nd systems were thermodynamically reoptimized. The calculated heat (absorbed or released) for all the invariant reactions agrees well with those from thermal measurement on a relative scale.

Acknowledgements

The authors would like to acknowledge financial support from the Multi-University Research Initiative (Grant No. F49602-01-1-0352) and from NDF Grant DMR-0111198 and in part from the Computational Materials Science Network, a program of the Office of Science, US Department of Energy. MCG is indebted to AD Rollett for his unlimited support during writing this manuscript. Also, MCG would like to thank C. Qiu for valuable discussion on Calphad data-base development and G. Cacciamani for providing assessed experimental data file for Al-Ce system and assessed databases of Al-Ce, Al-Nd and Al-La systems. We acknowledge inspiring and useful discussions with T.D. Massalski, Y. Wang and S.J. Poon.

References

1) Y. He, S.J. Poon, and G.J. Shiflet: Science, 1988, vol. 241, pp. 1640-42.

2) A. Inoue, K. Ohtera, and T. Masumoto: Jpn. J. Appl. Phys., 1988, vol. 27, pp. L736-39.

3) W. Biltz and H. Pieper: Z. Anorg. Chem., 1924, vol. 134, pp. 13.

4) G. Canneri and A. Rossi: Gazz. Chim. Ital., 1932, vol. 62, pp. 202-11.

5) J.H.N. van Vucht: Z. Metallk., 1957, vol. 48, pp. 253.

6) K.H.J. Buschow and J.H.N. van Vucht: Philips Res. Rep., 1965, vol. 20, pp. 337-48.

7) K.H.J. Buschow: J. Less-Com. Metals, 1965, vol. 9, pp. 452-56.

8) K.H.J. Buschow and J.H.N. van Vucht: Z. Metallk., 1966, vol. 57, pp. 162-66.

9) L.F. Yamshchikov, V.A. Lebedev, I.F. Nichkov, S.P. Raspopin, and O.K, Kokoulin: Izv. Vyssh Uchebn. Zaved., Tsvetn. MetaU., 1980, vol. 5, pp. 50-54.

10) V.I. Kononenko and S.V. Golubev: Izv. Akad Nauk SSSR, Met., 1990, vol. 2, pp. 197-99.

11) N. Clavaguera and Y. Du: J. Phase Equili., 1996, vol. 17, pp. 107-11.

12) J. Wang: Calphad, 1996, vol. 20, pp. 135-38.

13) G.B. Kale, A. Biswas, and I.G. Sharma: Scripta Mater., 1997, vol. 37, pp. 999-1003.

14) A.H. Gowes De Mesquita and K.H.J. Buschow: Acta Crystallogr., 1967, vol. 22, pp. 497-501.

15) M. Baricco, F. Gaetner, G. Cacciamani, P. Rizzi, L. Battezzati, and A.L. Greer: Mat. Sci. Forum, 1998, vol. 269-272, pp. 553-58.

16) L. Battezzati, M. Barcicco, and C. Antonione: J. Alloys. Comp., 1994, vol. 209, pp. 341-49.

17) A. Saccone, A.M. Cardinale, S. Delfino, and R. Ferro: Z. Metallk., 1996, vol. 87, pp. 82-87.

18) G. Cacciamani and R. Ferro: Calphad, 2001, vol. 25, pp. 583-97.

19) A.M. Cardinale, G. Cacciamani, G. Borzone, and R. Ferro: Calphad, 2003, vol. 27, pp.221-26.

20) G. Cacciamani., A.M. Cardinale, G. Borzone, and R. Ferro: Calphad, 2003, vol. 27, pp. 227-33.

21) K.A.Gschneidner Jr. and F.W.Calderwood: Bull. Alloy Phase Diagrams, 1988, vol. 9, pp. 669-72.

22) T. Godecke, W. Sun, R. Luck, and K. Lu: Z. Metallkd., 2001, vol. 92, pp. 723-30.

23) C. Colinet, A. Pasturel, and K.H.J. Buschow: J. Chem. Thermodyn., 1985, vol. 17, pp. 1133-139.

24) F. Sommer and M. Keita: J. Less-Com. Met., 1987, vol. 136, pp. 95-99.

25) G. Borzone, G.Cacciamani, and R. Ferro: Met. Trans., 1991, vol. 22A, pp. 2119-123.

26) G. Borzone, A.M. Cardinale, G. Cacciamani, and R. Ferro: Z. Metall., 1993, vol. 84, pp. 635-40.

27) B. Sundman, B. Jansson, and J.-O. Andersson: Calphad, 1985, vol. 9, pp. 153-90.

28) G. Kresse and J. Hafner: Phys. Rev. B, 1993, vol. 47, pp. 558-61.

29) G. Kresse and J. Furthmuller: Phys. Rev. B, 1996, vol. 54, pp. 11169-86.

30) G. Kresse and D. Joubert: Phys. Rev. B, 1999, vol. 59, pp. 1758-75.

31) J.P. Perdew, K. Burke, and M. Ermzerhoff: Phys. Rev. Lett., 1996, vol. 77, pp. 3865-68.

32) WWW site http://alloy.phys.cmu.edu (see special ‘‘published’’ entries).

33) M. Mihalkovic and M. Widom: Phys. Rev. B 70 (2004) 144107-19.

34) P. Villars, Pearson’s handbook, desk edition, ASM (1997).

35) M. Hillert and L.I. Staffanson: Acta Chem. Scand., 1970, vol. 24, pp. 3618-26.

36) A.T. Dinsdale: Calphad, 1991, vol. 15, pp. 317-425.

37) O. Redlich and A.T. Kister: Ind. Eng. Chem., 1948, vol. 40, pp. 345.

38) Y.M. Muggianu, M. Gambino, and J.P. Bros: J. Chim. Phys., 1975, vol. 22, pp. 83-88.

39) M. Hillert and M. Jarl: Calphad, 1978, vol. 2, pp. 227-38.

40) L. Kaufman, P. E. A. Turchi, W. Huang and Z.-K. Liu: Calphad, 2001, vol. 25, pp. 419-33.

41) C. Wolverton: Acta mater., 2001, vol. 49, pp. 3129-42.

42) C. Wolverton, X.-Y. Yan, R. Vijayaraghavan, and V. Ozolin: Acta mater., 2002, vol. 50, pp. 2187-97.

Table 1: Enthalpy of formation of stable compound phases, ΔH_{for}, (kJ/mole of atoms) at 0K for Al-Ce and Al-Nd systems calculated by first-principles.

Compound (type)	ΔH_f (Al-Ce)	ΔH_f (Al-Nd)
Al_4RE (tIl0)	-29.1480	-31.4637
$Al_{11}RE_3$ (oI28)	-34.6477	-36.0853
β-Al_3RE (hP12)	-38.4492	-38.0536
α-Al_3RE (hP8)	-40.9192	-38.7097
Al_2RE (cF24)	-44.5952	-49.5835
AlRE (oC16)	-32.5057	-39.5973
$AlRE_2$ (oP12)	-21.2170	-26.6587
β-$AlCe_3$ (cP4)	-15.0130	
α-$AlRE_3$ (hP8)	-15.7849	-26.9289

Table 2: Thermodynamic parameters for Al-Ce system optimized in this study (energy is in the unit of J/mole of atoms)

Phase	Parameters	Value
Liquid	${}^{o}L^{liquid}_{\mathrm{Al,Ce}}$	-130370.9+38.523T
	${}^{1}L^{liquid}_{\mathrm{Al,Ce}}$	-36330.4+6.362T
	${}^{2}L^{liquid}_{\mathrm{Al,Ce}}$	-9207.7+4.065T
fcc-A1	${}^{o}L^{fcc}_{\mathrm{Al,Ce}}$	-62850.9+30.556T
bcc-A2	${}^{o}L^{bcc}_{\mathrm{Al,Ce}}$	-93683+37.261T
Al_4Ce	$G^{Al_4Ce}_{\mathrm{Al:Ce}} - 0.8\,{}^{o}G^{fcc}_{Al} - 0.2\,{}^{o}G^{fcc}_{Ce}$	-29557+2.001T

Table 2: Thermodynamic parameters for Al-Ce system optimized in this study (energy is in the unit of J/mole of atoms)

Phase	Parameters	Value
$Al_{11}Ce_3$	$G^{\alpha Al_{11}Ce_3}_{\text{Al:Ce}} - 0.7857\,{}^{o}G^{fcc}_{Al} - 0.2143\,{}^{o}G^{fcc}_{Ce}$	-42745.1+11.159T
β-Al_3Ce	$G^{\beta Al_3Ce}_{\text{Al:Ce}} - 0.75\,{}^{o}G^{fcc}_{Al} - 0.25\,{}^{o}G^{fcc}_{Ce}$	-44437.2+9.867T
α-Al_3Ce	$G^{\alpha Al_3Ce}_{\text{Al:Ce}} - 0.75\,{}^{o}G^{fcc}_{Al} - 0.25\,{}^{o}G^{fcc}_{Ce}$	-45421+10.658T
Al_2Ce	$G^{Al_2Ce}_{\text{Al:Ce}} - 0.6667\,{}^{o}G^{fcc}_{Al} - 0.3333\,{}^{o}G^{fcc}_{Ce}$	-50060+9.889T
AlCe	$G^{AlCe}_{\text{Al:Ce}} - 0.5\,{}^{o}G^{fcc}_{Al} - 0.5\,{}^{o}G^{fcc}_{Ce}$	-48000+14.468T
$AlCe_2$	$G^{AlCe_2}_{\text{Al:Ce}} - 0.3333\,{}^{o}G^{fcc}_{Al} - 0.6667\,{}^{o}G^{fcc}_{Ce}$	-24816+0.714T
β-$AlCe_3$	$G^{\beta AlCe_3}_{\text{Al:Ce}} - 0.25\,{}^{o}G^{fcc}_{Al} - 0.75\,{}^{o}G^{fcc}_{Ce}$	-27935.2+9.816T
α-$AlCe_3$	$G^{\alpha AlCe_3}_{\text{Al:Ce}} - 0.25\,{}^{o}G^{fcc}_{Al} - 0.75\,{}^{o}G^{fcc}_{Ce}$	-28226+10.372T

Table 3: Thermodynamic parameters for Al-Nd system obtained in this study (energy is in the unit of J/mole of atoms)

Phase	Parameters	Value
Liquid	${}^{o}L^{liquid}_{\text{Al,Nd}}$	-159238.1+57.514T
	${}^{1}L^{liquid}_{\text{Al,Nd}}$	-1349.7-25.797T
	${}^{2}L^{liquid}_{\text{Al,Nd}}$	24298.7-25.299T
bcc-A2	${}^{o}L^{bcc}_{\text{Al,Nd}}$	-150515.5+47.415T
	${}^{1}L^{bcc}_{\text{Al,Nd}}$	-36877.5

Table 3: Thermodynamic parameters for Al-Nd system obtained in this study (energy is in the unit of J/mole of atoms)

Phase	Parameters	Value
dhcp	${}^{o}L^{dhcp}_{\mathrm{Al,Nd}}$	-132036.2+28.661T
	${}^{1}L^{dhcp}_{\mathrm{Al,Nd}}$	-61093.6
Al_4Nd	$G^{Al_4Nd}_{\mathrm{Al:Nd}} - 0.8\,{}^{o}G^{fcc}_{Al} - 0.2\,{}^{o}G^{dhcp}_{Nd}$	-30096.9+1.365T
$Al_{11}Nd_3$	$G^{Al_{11}Nd_3}_{\mathrm{Al:Nd}} - 0.7857\,{}^{o}G^{fcc}_{Al} - 0.2143\,{}^{o}G^{dhcp}_{Nd}$	-39354.7+7.72T
β-Al_3Nd	$G^{\beta Al_3Nd}_{\mathrm{Al:Nd}} - 0.75\,{}^{o}G^{fcc}_{Al} - 0.25\,{}^{o}G^{dhcp}_{Nd}$	-43229.1+8.022T
α-Al_3Nd	$G^{\alpha Al_3Nd}_{\mathrm{Al:Nd}} - 0.75\,{}^{o}G^{fcc}_{Al} - 0.25\,{}^{o}G^{dhcp}_{Nd}$	-45046.4+9.587T
Al_2Nd	$G^{Al_2Nd}_{\mathrm{Al:Nd}} - 0.6667\,{}^{o}G^{fcc}_{Al} - 0.3333\,{}^{o}G^{dhcp}_{Nd}$	-54036.7+11.622T
AlNd	$G^{AlNd}_{\mathrm{Al:Nd}} - 0.5\,{}^{o}G^{fcc}_{Al} - 0.5\,{}^{o}G^{dhcp}_{Nd}$	-51109.7+15.354T
$AlNd_2$	$G^{AlNd_2}_{\mathrm{Al:Nd}} - 0.3333\,{}^{o}G^{fcc}_{Al} - 0.6667\,{}^{o}G^{dhcp}_{Nd}$	-35857.7+10.073T
$AlNd_3$	$G^{AlNd_3}_{\mathrm{Al:Nd}} - 0.25\,{}^{o}G^{fcc}_{Al} - 0.75\,{}^{o}G^{dhcp}_{Nd}$	-27788.3+ 7.208T

FIGURE CAPTIONS

Figure 1: Al-Ce (a) and Al-Nd (b) binary phase diagrams assessed by Cacciamani and Ferro [18].

Figure 2: DTA plots for alloys (a) $Al_{97.4}Ce_{2.6}$; (b) $Al_{82.5}Ce_{17.5}$ at heating and cooling rates of 20 ^{o}C/min. It can be concluded that (a) is a eutectic alloy, and that 3 reactions occur in (b). The spike that occurs at ~1350^{o}C in (b) is an artificial signal from the DTA unit.

Figure 3: DTA plots for (a) $Al_{40}Ce_{60}$; (b) $Al_{30}Ce_{70}$; (c) $Al_{20}Ce_{80}$; (d) $Al_{25}Ce_{75}$ at a heating rate of 20 ^{o}C/min. The inset is the first peak of (d) $Al_{25}Ce_{75}$, where two tightly overlapping peaks, marked by the arrows, correspond to the reactions of $\beta AlCe_3 + AlCe \leftrightarrow AlCe_2$ and $\beta AlCe_3 \leftrightarrow AlCe_2 + Liquid$. The bulk chemistry of (d) is slightly shifted from their norminal value to the Al-rich side.

Figure 4a: DSC plot for $Al_{11}Nd_3$ at a heating rate of 20 K/min (done with Netzsch DSC 404). There are 2 peaks present in the mediate temperature regime marked by the arrows, which correspond to the reactions of $Liquid + Al_{11}Nd_3 \leftrightarrow Al_4Nd$ and $Al_{11}Nd_3 \leftrightarrow \beta Al_3Nd + Al_4Nd$. They can be regarded as direct evidence supporting that the so-called $\beta-Al_{11}RE_3$ [7,8,21,22] should be treated as Al_4RE (RE=La,Ce,Nd,Pr) phase. The insets are the first derivative of the peak, which might imply of two overlapping reactions, namely $Al_2Nd + Al_4Nd \leftrightarrow \beta Al_3Nd$ and $Al_2Nd + Liquid \leftrightarrow Al_4Nd$.

Figure 4b: DTA plot for alloy $Al_{76}Nd_{24}$ at a heating/cooling rate of 10 K/min (done with PerkinElmer DTA 7). The arrow indicates the α/β-Al_3Nd polymorphous transformation occurring at 888^{o}C. It can be clearly seen that the reactions of $Al_2Nd + Al_4Nd \leftrightarrow \beta Al_3Nd$ and $Al_2Nd + Liquid \leftrightarrow Al_4Nd$ indeed overlap, and the heat from the latter is significantly larger than that from the former. The reaction of $Al_{11}Nd_3 \leftrightarrow \beta Al_3Nd + Al_4Nd$ is not detected in this scan, and the reason can be due to small amount of heat and slow kinetics for this reaction.

Figure 4c: DTA plot for alloy $Al_{75}Ce_{25}$ at a heating/cooling rate of 10 K/min (done with PerkinElmer DTA 7). The arrow indicates the α/β-Al_3Ce polymorphous transformation occurring at ~973^{o}C. The second peak during heating corresponds to the reaction of $Al_2Ce + Al_4Ce \leftrightarrow \beta Al_3Ce$, and the third peak corresponds to the reaction of $Al_2Ce + Liquid \leftrightarrow Al_4Ce$. Note the final melting peak is very broad and that the first peak has a small amount of heat.

Figure 5: Back-scattering SEM micrographs of alloy $Al_{40}Ce_{60}$ after annealed at (a) 700^{o}C, (b) 500^{o}C and (c) 200^{o}C for 10 days. Three phases are present in (a) and (b), i.e. AlCe, α-

$AlCe_3$ and β-$AlCe_3$. There are a significant amount of β-$AlCe_3$ in (a) but very little in (b). Only AlCe and α-$AlCe_3$ are present in (c). The $AlCe_2$ phase is not retained in the microstructure after annealing at 700°C for 10 days followed by quenching in cold water.

Figure 6: Cohesive energy plots for (a) Al-Nd and (b) Al-Ce systems calculated at 0K using VASP program. Refer to Table 1 for the exact values of cohesive energy of compound phases.

Figure 7: Calculated Al-Ce binary phase diagram via CALPHAD method based on present study and literature information. The experimental thermal events are marked for comparison. The invariant temperatures marked on the phase diagram are obtained from experimental reports.

Figure 8a: Calculated heat of mixing of Al-Ce alloys at 300K via CALPHAD method based on the present study and literature information. The formation enthalpy of Al-Ce compound phases that was reported in the literature are marked for comparison, together with those calculated from first-principles in this study (see Table 1).

Figure 8b: Calculated enthalpy evolution of alloys $Al_{40}Ce_{60}$ and $Al_{70}Ce_{30}$ vs. temperatures. The first-order phase transition is recognized by the vertical discontinuity in enthalpy at the transition temperature (marked by the dotted lines), which is the heat associated for the reaction. The calculated total enthalpy change for each invariant reaction is seen in good agreement with those obtained from DTA measurement for the same alloy (see Fig. 3) on a relative scale. The phase field separated by the invariant temperatures are also marked.

Figure 9: Calculated Al-Nd binary phase diagram via CALPHAD method based on the present study and available literature information with experimental thermal events marked for comparison. The invariant temperatures determined from experiments are also marked.

Figure 10a: Calculated heat of mixing of Al-Nd alloys at 300K via CALPHAD method based on the present study and available literature information. The formation enthalpy of Al-Nd compound phases that were reported in [26] are marked for comparison together with those calculated from first-principles in this study (see Table 1).

Figure 10b: Calculated total enthalpy evolution of alloys $Al_{79.5}Nd_{20.5}$ and $Al_{76}Nd_{24}$ vs. temperatures. The first-order phase transition is recognized by the vertical discontinuity in enthalpy at the transition temperature (marked by the dotted lines), which is the heat associated for the reaction. The calculated total enthalpy change for each invariant reaction is seen in good agreement with the heat obtained from DTA measurement for the same alloy (see Fig. 4) on a relative scale. The phase field separated by the invariant temperatures are also marked.

Figure 1.

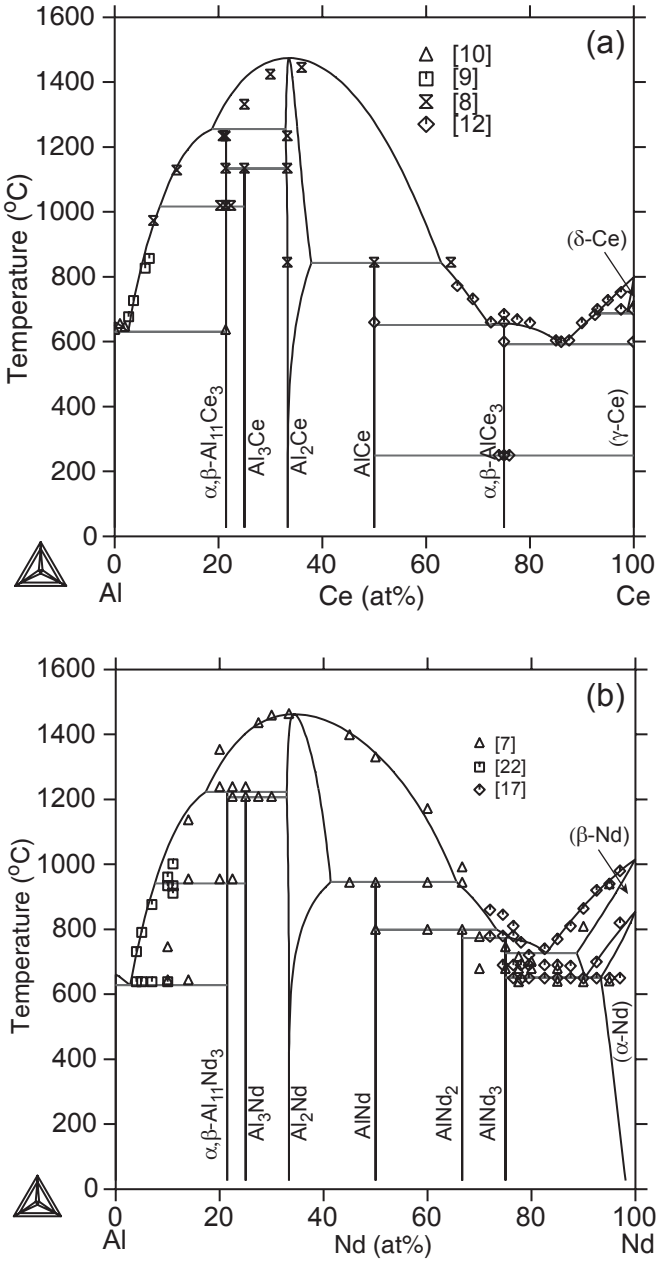
(a)
[10]
[9]
[8]
[12]
(δ-Ce)
(γ-Ce)
α,β-Al11Ce3
Al3Ce
Al2Ce
AlCe
α,β-AlCe3
Temperature (°C)
Al
Ce (at%)
Ce
(b)
[7]
[22]
[17]
(β-Nd)
(α-Nd)
α,β-Al11Nd3
Al3Nd
Al2Nd
AlNd
AlNd2
AlNd3
Temperature (°C)
Al
Nd (at%)
Nd

Figure 2.

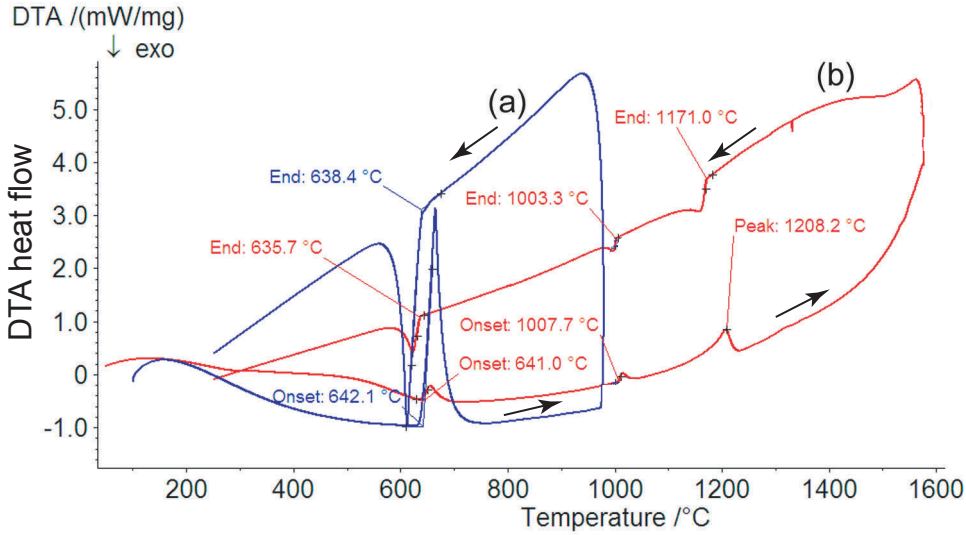

Figure 3 (a)-(d)

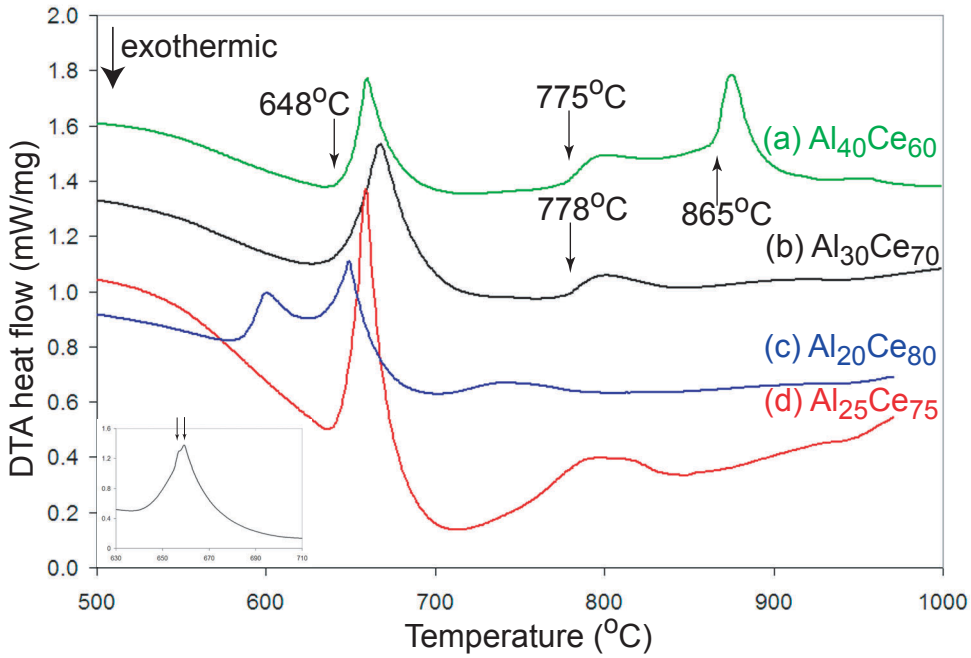

Figure 4 (a)

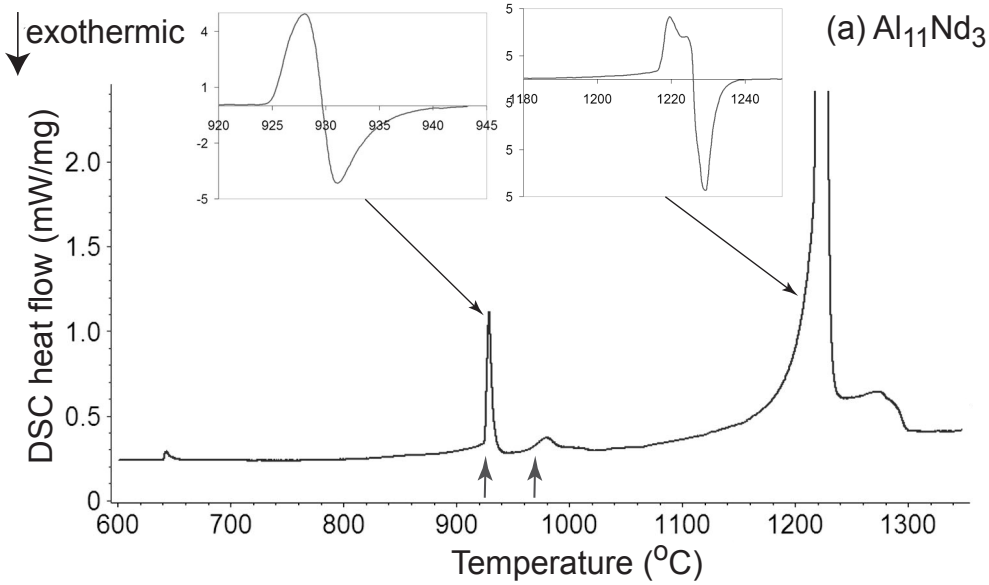

Figure 4b.

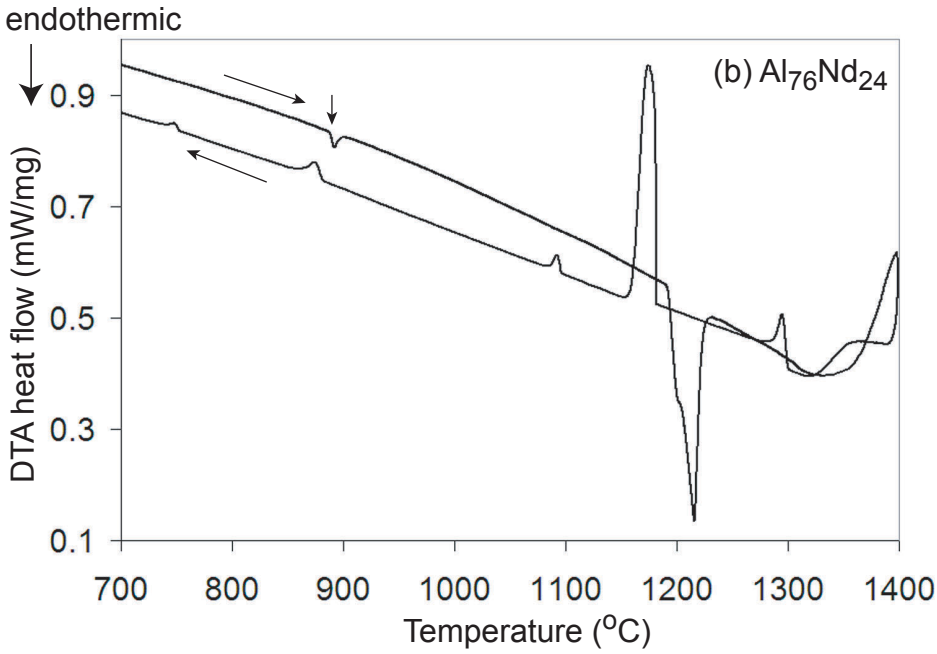

Figure 4c.

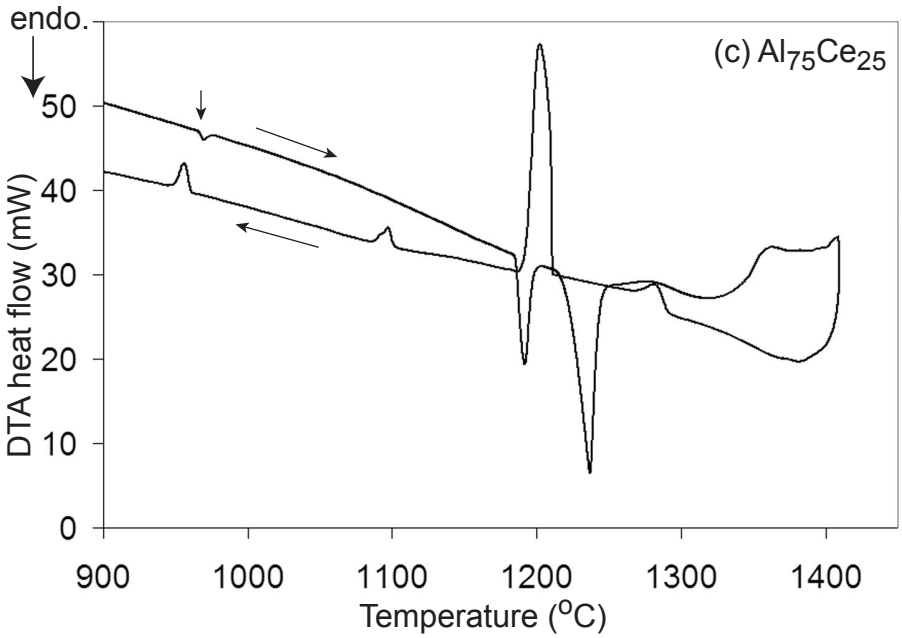
endo.
(c) $Al_{75}Ce_{25}$
DTA heat flow (mW)
0
10
20
30
40
50
900
1000
1100
1200
1300
1400
Temperature (^{o}C)

Figure 5.

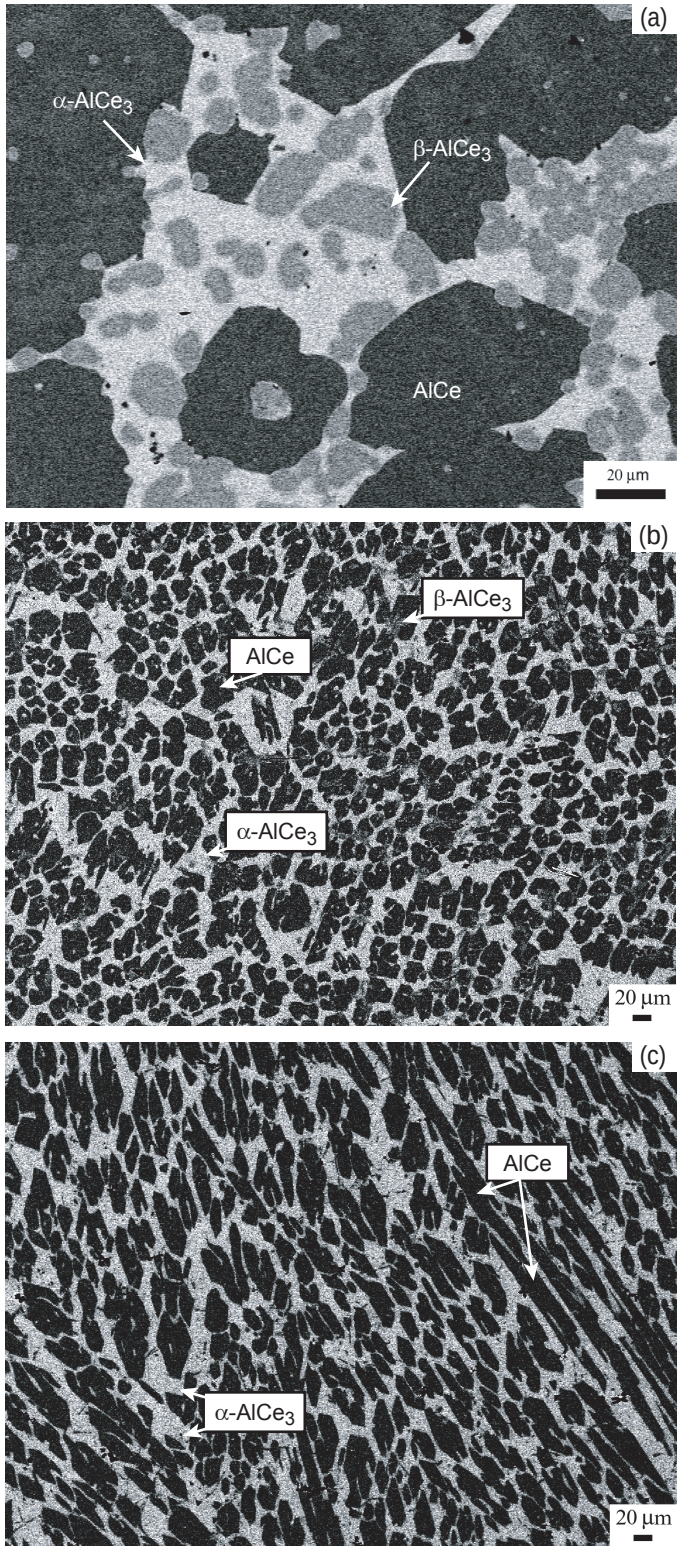
(a)
α-AlCe3
β-AlCe3
AlCe
20 μm
(b)
β-AlCe3
AlCe
α-AlCe3
20 μm
(c)
AlCe
α-AlCe3
20 μm

Figure 6a

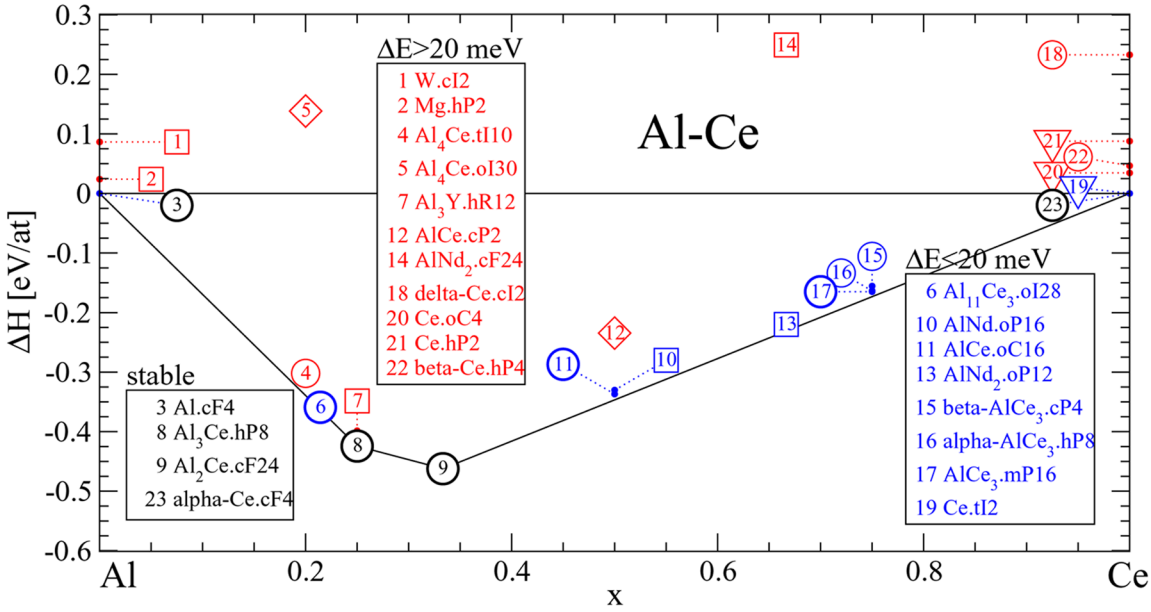

Figure 6b

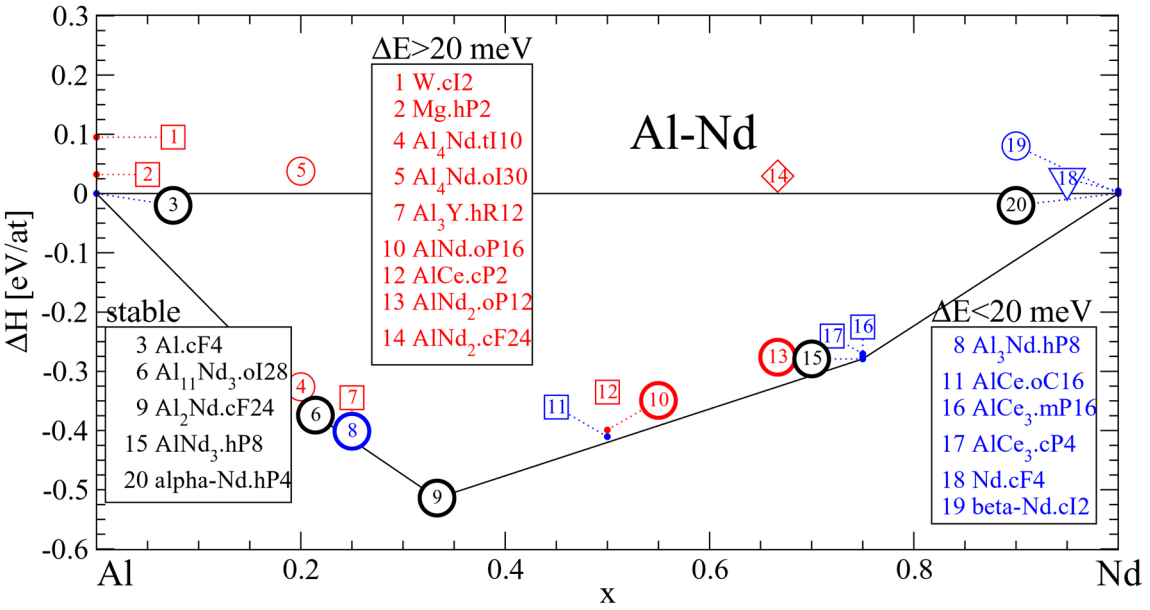

Figure 7

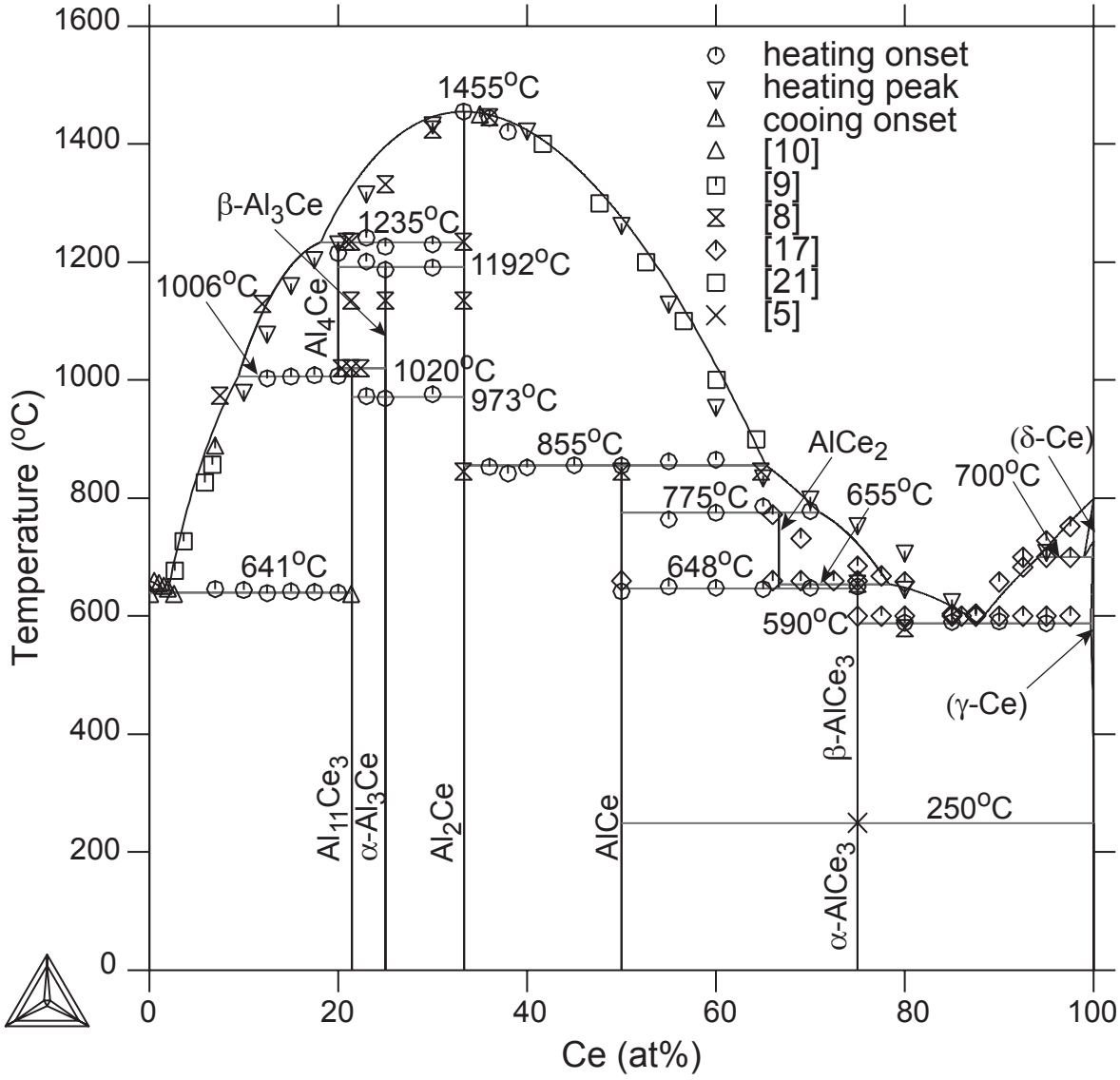
heating onset
heating peak
cooing onset
[10]
[9]
[8]
[17]
[21]
[5]
1455°C
β-Al3Ce
1235°C
1192°C
1006°C
Al4Ce
1020°C
973°C
855°C
AlCe2
(δ-Ce)
700°C
775°C
655°C
641°C
648°C
590°C
(γ-Ce)
β-AlCe3
Al11Ce3
α-Al3Ce
Al2Ce
AlCe
250°C
α-AlCe3
Temperature (°C)
Ce (at%)
0
200
400
600
800
1000
1200
1400
1600
0
20
40
60
80
100

Figure 8a.

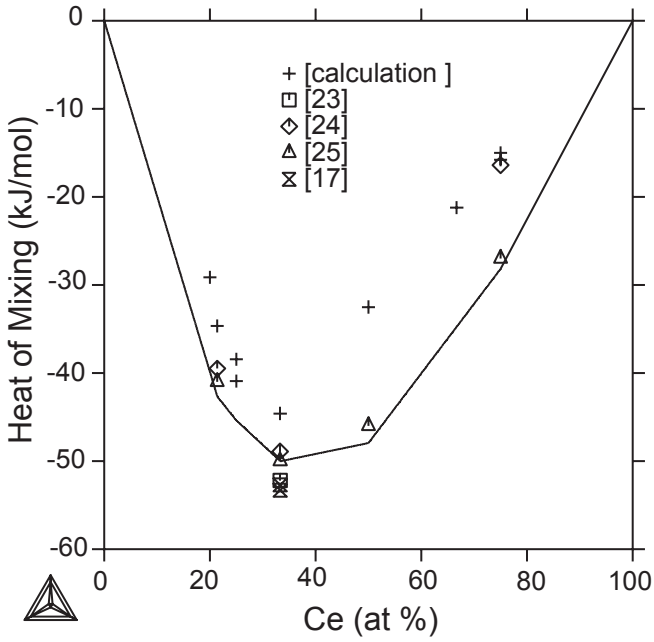

Figure 8b

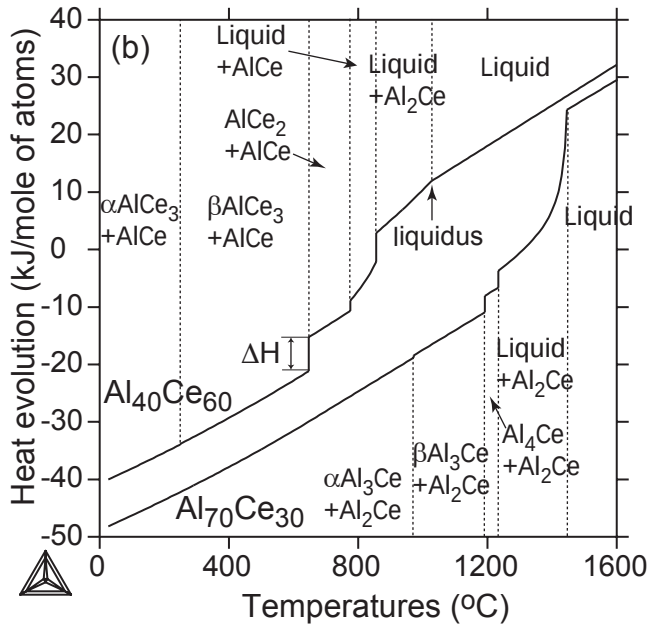

Figure 9.

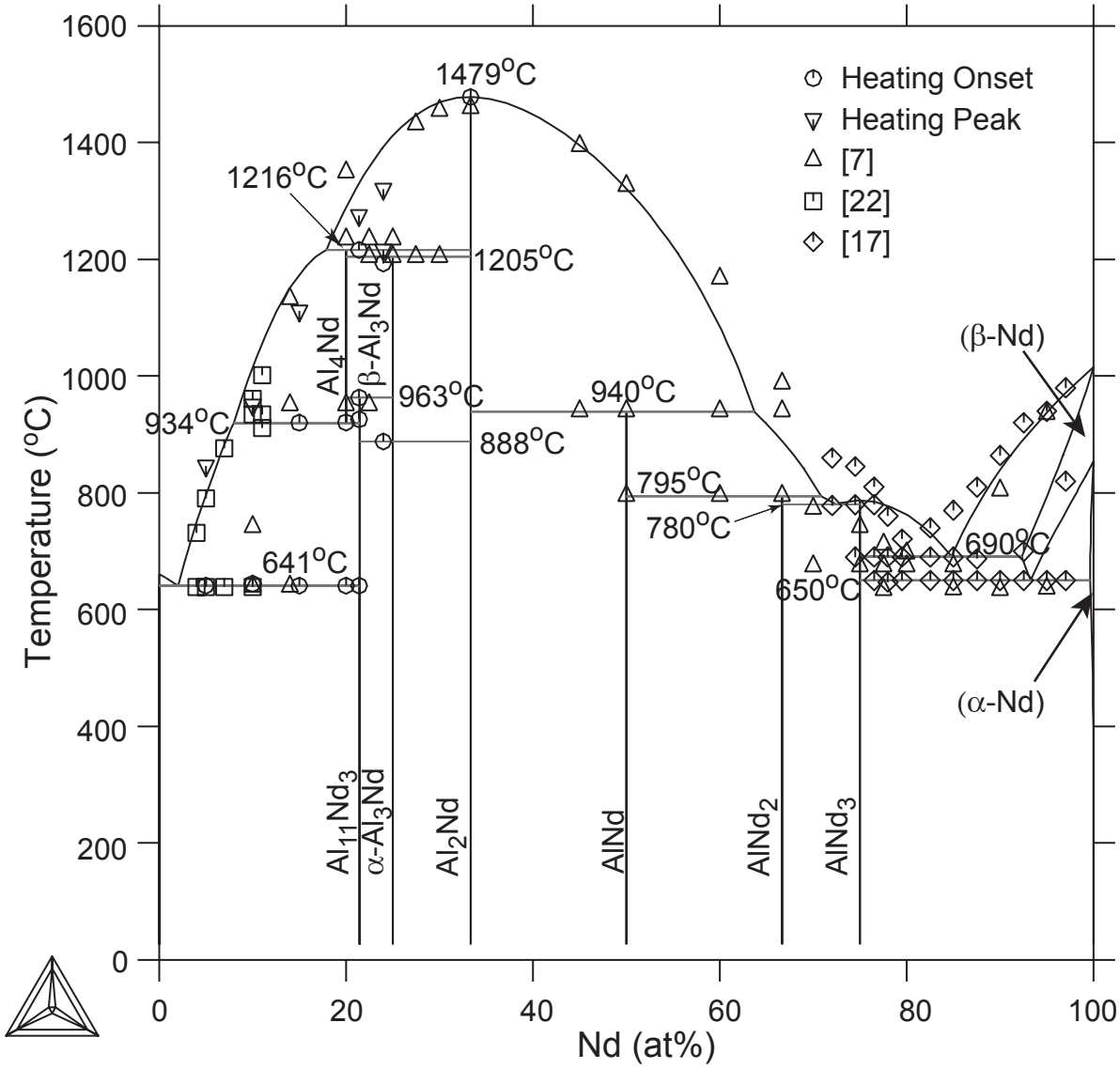
1600
1400
1200
1000
800
600
400
200
0
Temperature (°C)
0
20
40
60
80
100
Nd (at%)
1479°C
1216°C
1205°C
963°C
940°C
934°C
888°C
795°C
780°C
690°C
650°C
641°C
Heating Onset
Heating Peak
[7]
[22]
[17]
(β-Nd)
(α-Nd)
Al4Nd
β-Al3Nd
Al11Nd3
α-Al3Nd
Al2Nd
AlNd
AlNd2
AlNd3

Figure 10a

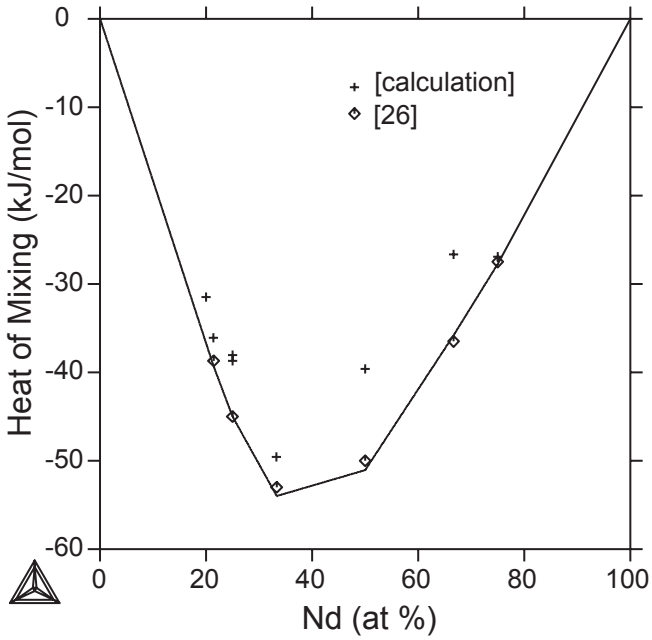

Figure 10b